Published in final edited form as:
Science. 2020 July 31; 369(6503): 554–557. doi:10.1126/science.abb3758.

In-cell architecture of an actively transcribing-translating expressome*

Francis J. O'Reilly[#1], **Liang Xue**[#2,3], **Andrea Graziadei**[#1], **Ludwig Sinn**[1], **Swantje Lenz**[1], **Dimitry Tegunov**[4], **Cedric Blötz**[5], **Neil Singh**[5], **Wim J. H. Hagen**[2], **Patrick Cramer**[4], **Jörg Stülke**[5], **Julia Mahamid**[2,*], **Juri Rappsilber**[1,6,*]

[1]Bioanalytics Unit, Institute of Biotechnology, Technische Universität Berlin, 13355 Berlin, Germany

[2]Structural and Computational Biology Unit, European Molecular Biology Laboratory (EMBL), Meyerhofstraße 1, 69117 Heidelberg, Germany

[3]Collaboration for joint PhD degree between EMBL and Heidelberg University, Faculty of Biosciences

[4]Department of Molecular Biology, Max-Planck-Institute for Biophysical Chemistry, Am Faßberg 11, 37077, Göttingen, Germany

[5]Department of General Microbiology, Institute of Microbiology and Genetics, GZMB, Georg-August-University Göttingen, Grisebachstraße 8, 37077 Göttingen, Germany

[6]Wellcome Centre for Cell Biology, University of Edinburgh, Max Born Crescent, Edinburgh, EH9 3BF, UK

[#] These authors contributed equally to this work.

Abstract

Structural biology performed inside cells can capture molecular machines in action within their native context. Here we developed an integrative in-cell structural approach using the genome-reduced human pathogen *Mycoplasma pneumoniae.* We combined whole-cell crosslinking mass spectrometry, cellular cryo-electron tomography, and integrative modeling to determine an in-cell

*Correspondence to: julia.mahamid@embl.de, juri.rappsilber@tu-berlin.de.

Author contributions: F.O., L.X., J.M. and J.R. designed the experiments; F.O., L.S. and S.L. collected and processed CLMS data; C.B. and J.S. performed the bacterial two-hybrid work; N.S. performed mutation experiments; L.X. and J.M. collected and processed cryo-EM data; W.H. supported cryo-EM data collection; D.T. and P.C. contributed new cryo-EM processing software; A.G. and S.L performed integrative modelling; F.O., L.X., A.G., J.M. and J.R. prepared figures and wrote the manuscript with inputs from all authors.

Competing interests: The authors have no competing interests.

Data and materials availability: The Supplementary Materials contain additional data. EM densities have been deposited in the EMDataBank with the following accession numbers: EMD-10677,10678, 10679, 10680, 10681, 10682, 10683, 10684, 10685, 10686, 10687. CLMS data are available via ProteomeXchange with identifiers PXD017711 (DSSo) and PXD017695 (DSS). The integrative model is available in PDB-Dev with accession number PDBDEV_00000049. Homology models are available at the ModelArchive with accession codes: ma-mrryl, ma-7ov95, ma-eeo9f, ma-8tn6v. Integrative modeling code and raw files are available in Zenodo under the doi https://doi.org/10.5281/zenodo.3829334.

Europe PMC Funders Author Manuscripts

architecture of a transcribing and translating expressome at sub-nanometer resolution. The expressome comprises RNA polymerase (RNAP), the ribosome, and the transcription elongation factors NusG and NusA. We pinpointed NusA at the interface between a NusG-bound elongating RNAP and the ribosome, and propose it can mediate transcription-translation coupling. Translation inhibition dissociated the expressome, whereas transcription inhibition stalled and rearranged it. Thus, the active expressome architecture requires both translation and transcription elongation within the cell.

The two fundamental processes of gene expression, transcription and translation, are functionally coupled in bacteria. While the transcribing RNA polymerase (RNAP) produces a nascent mRNA chain that can be directly translated by ribosomes (1–3), translation was shown to influence the overall transcription rate in *Escherichia coli* (4, 5), implying a physical link between the two processes. Accordingly, an in vitro-reconstituted *E. coli* RNAP-ribosome supercomplex structure was determined and termed "expressome" (6). Additional in vitro reconstitutions, some including the essential factor NusG (7) that is proposed to link RNAP and the ribosome (8, 9), reveal different structural arrangements of the supercomplex (10–12). These raise questions as to the mechanisms of coupling that could be utilized inside the cell, in the context of all regulatory factors.

To structurally analyze transcription-translation coupling inside cells, we combined in-cell crosslinking mass spectrometry (CLMS) (13) and cellular cryo-electron tomography (cryo-ET) (14). We used the small genome-reduced bacterium *Mycoplasma pneumoniae*, which is an ideal cell model for system-wide structural studies (15). While *M. pneumoniae* has undergone significant genome reduction during its evolution as a human pathogen, it has retained the core transcription and translation machineries (16–18).

To assess the topology of a putative RNAP-ribosome supercomplex and its associated regulatory factors, we performed whole-cell CLMS of intact *M. pneumoniae* cells (13, 19) (fig. S1 and table S1). We identified 10,552 crosslinks involving the same protein (self-links) and 1957 heteromeric crosslinks with a 5% residue-pair false discovery rate (FDR). These represented 577 distinct protein-protein-interactions (PPIs) at a 5% PPI-FDR (Fig. 1A and supplementary text). Identified crosslinks covered 83% of the detectable proteome (table S2 and fig. S1), including PPIs of membrane proteins (41% of PPIs), 76 uncharacterized proteins, the ribosome, RNAP and their associated factors (Fig. 1B and fig. S1-S3).

The *M. pneumoniae* RNAP core consisting of the conserved subunits α, β and β', was found to interact with the known auxiliary factors SigA, GreA, NusG, NusA, SpxA, and RpoE (firmicute-specific RNAP δ subunit) (20) (Fig. 1B). Additionally, two uncharacterized essential proteins, MPN555 and MPN530 (21), were found and the interaction of MPN530 with β/β' subunits was independently validated by a bacterial two-hybrid screen (fig. S4). Despite these interactions, no direct crosslinks between the RNAP core and the ribosome were identified. Interaction between NusG and the ribosomal protein S10, previously reported in *E. coli*, was also not detected (8, 9). Instead, NusA, an essential transcription factor involved in elongation, termination and antitermination (21–23), was found to interact with RNAP via its N-terminal domain (NTD), and with the mRNA entry site of the

ribosome via its C-terminal region (Fig. 1B). In-cell CLMS thus indicated an unexpected architecture in which RNAP and the ribosome are linked by NusA.

To investigate the structure of this potential association, cryo-ET data were acquired on unperturbed, frozen-hydrated *M. pneumoniae* cells (19) (Fig. 2A and fig. S5). 108,501 ribosome sub-tomograms were extracted and subjected to classification and refinement (fig. S6, S7). These exhibited large structural heterogeneity and were first sorted into classes representing the 50S subunit (30.3%), 70S ribosomes (53.3%) and 70S ribosomes in the closely-assembled polysome configuration (24) (16.4%) (Fig. 2A and fig. S7). Subjecting 73,858 70S ribosomes to a new subtomogram analysis workflow (fig. S6) (19) resulted in a 5.6 Å ribosome density (Fig. 2B, fig. S8). A ribosome homology model (based on PDB 3J9W) was fitted and the majority of *M. pneumoniae* ribosomal proteins could be mapped (fig. S9). Helical densities at the C-termini of L22 and L29 (Fig. 2B, insert) were unaccounted for by the homology model and assigned to two C-terminal extensions that are unique to *M. pneumoniae* and its close relatives (fig. S10 and S11). L23, which also contains a C-terminal extension, was predicted to be unstructured and did not produce any discernible density in the map (fig. S12). Therefore, in conjunction with CLMS, the attained high-resolution map enabled de novo assignment of secondary structures in cellulo.

Focused classification of the 70S on the mRNA entry site identified a ribosome class in complex with RNAP (70S+RNAP, Fig. 2A and fig. S7). Refinement thereof provided a 9.2 Å map (fig. S13) into which the ribosome and RNAP models fitted unambiguously (Fig. 2C). Consistent with the CLMS data, the map contained additional density at the interface between the two complexes (Fig. 2C, arrowheads), which was further resolved by multi-body refinement (fig. S14). The path of the DNA and RNA-DNA hybrid duplex showed that RNAP is in an elongating state (Fig. 3A and fig. S15C). The existence of elongating RNAP and 70S ribosome demonstrated that the supercomplex represents an actively elongating expressome with a large degree of structural flexibility (Movie S1).

Both CLMS and cryo-EM results showed binding of NusG to its conserved site (fig. S15, S16) (25). *M. pneumoniae* NusG contains large inserts of unknown structure, but retains the residues involved in the NusG-S10 interaction (8). However, the arrangement of RNAP relative to the ribosome placed NusG away from S10, indicating that this interaction does not occur in the elongating expressome (fig. S16). All other proteins found interacting with RNAP by CLMS did not fit in the elongating expressome density (fig. S17). The remaining density between RNAP and the ribosome was therefore consistent with NusA (Fig. 1B and fig. S18).

The CLMS and cryo-EM data were used to derive an integrative model of the elongating expressome (26, 19) (fig. S19, table S4 and S5). *M. pneumoniae* NusA contains a disordered proline-rich C-terminal region that is not found in *E. coli* or *B. subtilis* (fig. S18), which we established to be essential by mutation experiments (fig. S20). This region, which was found to be crosslinked to multiple 30S ribosomal proteins (Fig.1B), was coarse-grained and not fitted into the density. The best scoring solutions (fig. S21) showed that the NusA NTD and S1 domain bind RNAP similarly to the *E. coli* paused elongation complex (23), with the S1 domain near the RNAP mRNA exit tunnel (Fig. 3B,C and fig. S22). The two KH domains

were positioned near S3, S4 and S5 at the ribosome mRNA entry site. The orientation of KH domains retained their RNA-binding interface in a position that can interact with the nascent mRNA (27) (fig. S23). The C-terminal domains (CTDs) of RNAP α subunits were found to be in a wide range of conformations localized between NusA NTD and the second KH domain, with one α-CTD fitting a region between the second NusA KH domain and the RNAP core (fig. S23 and supplementary text). Additionally, the firmicute-specific RNAP δ subunit was positioned below RNAP β' CTD (fig. S24), consistent with its suggested role in regulating RNAP-DNA interactions (20).

The integrative model demonstrated that NusA bridges the elongating RNAP and ribosome in the active expressome. To determine whether this architecture requires active translation elongation, we collected cryo-ET data on cells treated with the translation inhibitor chloramphenicol (Cm). The percentage of 70S ribosomes increased dramatically compared to untreated cells (Fig. 4A and fig. S25). The resulting 6.5 Å ribosome density (Fig. 4B) had well-resolved A and P site tRNAs similar to a previous ribosome-Cm structure (28) (Fig. 4C), but do not contain any RNAP density near the ribosome mRNA entry site. Thus, stalling ribosomes led to dissociation of the expressome.

The dependence on active transcription was probed by treating cells with the specific RNAP inhibitor pseudouridimycin (PUM) (29), which significantly increased the percentage of well-resolved expressomes (Fig. 4A). The PUM-induced expressome was refined to 7.1 Å (fig. S26, 27 and Movie S2), revealing direct interaction between the NusG-bound RNAP and the ribosome, and excluding density for NusA (Fig. 4B and fig. S28). This stalled expressome closely resembled the architecture of the *E. coli* expressome solved in vitro (6) (fig. S28). Interestingly, tRNAs in the ribosome were found in hybrid A/P* and P/E states, and density corresponding to EF-G was well-resolved (Fig. 4C). This suggested that the ribosome was trapped in a pre-translocation state (fig. S28) (30), unable to complete the translocation step, presumably owing to physical obstruction by the stalled RNAP.

In summary, we have determined the native architecture of the expressome in *M. pneumoniae* and have shown that it requires active transcription and translation elongation. At the RNAP-ribosome interface we unexpectedly found NusA, which followed the path of nascent mRNA at the nexus of transcription-translation coupling. NusA may act as a sensor of RNAP that detects an approaching ribosome and modulates transcription elongation. However, it remains to be seen whether the involvement of NusA in the *M. pneumoniae* active expressome represents a feature that is conserved across bacteria. Our data highlight the structural heterogeneity of the process, and the potential of integrative in-cell structural biology in elucidating dynamic machineries within their native functional context.

Supplementary Material

Refer to Web version on PubMed Central for supplementary material.

Acknowledgments

We are grateful to Mahmoud Chaabou, Helena Barysz, Zhuo Angel Chen, Lutz Fischer, Colin Combe, Martin Graham, and Ievgeniia Zagoriy. Jan Kosinski, Christoph Müller and Martin Beck are acknowledged for critical reading of the manuscript.

Funding

This project received funding from the Deutsche Forschungsgemeinschaft under Germany's Excellence Strategy – EXC 2008/1 – 390540038, project no. 426290502 and 392923329, the Wellcome Trust Senior Research Fellowship (103139) to J.R., EMBL and the European Research Council to J.M. (760067) and to P.C. (693023). The Wellcome Centre for Cell Biology is supported by core funding from the Wellcome Trust (203149).

References

1. Santangelo TJ, Artsimovitch I. Termination and antitermination: RNA polymerase runs a stop sign. Nat Rev Microbiol. 2011; 9:319–329. [PubMed: 21478900]
2. McGary K, Nudler E. RNA polymerase and the ribosome: the close relationship. Curr Opin Microbiol. 2013; 16:112–117. [PubMed: 23433801]
3. Conn AB, Diggs S, Tam TK, Blaha GM. Two Old Dogs, One New Trick: A Review of RNA Polymerase and Ribosome Interactions during Transcription-Translation Coupling. Int J Mol Sci. 2019; 20:E2595. [PubMed: 31137816]
4. Landick R, Carey J, Yanofsky C. Translation activates the paused transcription complex and restores transcription of the trp operon leader region. Proc Natl Acad Sci U S A. 1985; 82:4663–4667. [PubMed: 2991886]
5. Proshkin S, Rahmouni AR, Mironov A, Nudler E. Cooperation between translating ribosomes and RNA polymerase in transcription elongation. Science. 2010; 328:504–508. [PubMed: 20413502]
6. Kohler R, Mooney RA, Mills DJ, Landick R, Cramer P. Architecture of a transcribing-translating expressome. Science. 2017; 356:194–197. [PubMed: 28408604]
7. Mooney RA, Davis SE, Peters JM, Rowland JL, Ansari AZ, Landick R. Regulator trafficking on bacterial transcription units in vivo. Mol Cell. 2009; 33:97–108. [PubMed: 19150431]
8. Burmann BM, Schweimer K, Luo X, Wahl MC, Stitt BL, Gottesman ME, Rösch P. A NusE:NusG complex links transcription and translation. Science. 2010; 328:501–504. [PubMed: 20413501]
9. Washburn RS, Zuber PK, Sun M, Hashem Y, Shen B. Escherichia coli NusG links the lead ribosome with the transcription elongation complex. bioRxiv.
10. Wang C, Molodtsov V, Firlar E, Kaelber J, Blaha G. Structural basis of transcription-translation coupling. bioRxiv.
11. Webster MW, Takacs M, Zhu C, Vidmar V, Eduljee AD. Structural basis of transcription-translation coupling and collision in bacteria. bioRxiv.
12. Demo G, Rasouly A, Vasilyev N, Svetlov V, Loveland AB, Diaz-Avalos R, Grigorieff N, Nudler E, Korostelev AA. Structure of RNA polymerase bound to ribosomal 30S subunit. elife. 2017; 6:e28560. [PubMed: 29027901]
13. O'Reilly FJ, Rappsilber J. Cross-linking mass spectrometry: methods and applications in structural, molecular and systems biology. Nat Struct Mol Biol. 2018; 25:1000–1008. [PubMed: 30374081]
14. Beck M, Baumeister W. Cryo-Electron Tomography: Can it Reveal the Molecular Sociology of Cells in Atomic Detail? Trends Cell Biol. 2016; 26:825–837. [PubMed: 27671779]
15. Kühner S, van Noort V, Betts MJ, Leo-Macias A, Batisse C, Rode M, Yamada T, Maier T, Bader S, Beltran-Alvarez P, Castaño-Diez D, et al. Proteome organization in a genome-reduced bacterium. Science. 2009; 326:1235–1240. [PubMed: 19965468]
16. Güell M, van Noort V, Yus E, Chen W-H, Leigh-Bell J, Michalodimitrakis K, Yamada T, Arumugam M, Doerks T, Kühner S, Rode M, et al. Transcriptome complexity in a genome-reduced bacterium. Science. 2009; 326:1268–1271. [PubMed: 19965477]
17. Grosjean H, Breton M, Sirand-Pugnet P, Tardy F, Thiaucourt F, Citti C, Barré A, Yoshizawa S, Fourmy D, de Crécy-Lagard V, Blanchard A, et al. Predicting the minimal translation apparatus:

lessons from the reductive evolution of mollicutes. PLoS Genet. 2014; 10:e1004363. [PubMed: 24809820]

18. Yus E, Lloréns-Rico V, Martínez S, Gallo C, Eilers H, Blötz C, Stülke J, Lluch-Senar M, Serrano L. Determination of the Gene Regulatory Network of a Genome-Reduced Bacterium Highlights Alternative Regulation Independent of Transcription Factors. Cell Syst. 2019; 9:143–158.e13. [PubMed: 31445891]
19. See supplementary materials
20. Weiss A, Shaw LN. Small things considered: the small accessory subunits of RNA polymerase in Gram-positive bacteria. FEMS Microbiol Rev. 2015; 39:541–554. [PubMed: 25878038]
21. Lluch-Senar M, Delgado J, Chen W, Lloréns-Rico V, O'Reilly FJ, Wodke JAH, Besray Unal E, Yus E, Martínez S, Nichols RJ, Ferrar T, et al. Defining a minimal cell: essentiality of small ORFs and ncRNAs in a genome-reduced bacterium. Mol Syst Biol. 2015; 11:780. [PubMed: 25609650]
22. Yang X, Molimau S, Doherty GP, Johnston EB, Marles-Wright J, Rothnagel R, Hankamer B, Lewis RJ, Lewis PJ. The structure of bacterial RNA polymerase in complex with the essential transcription elongation factor NusA. EMBO Rep. 2009; 10:997–1002. [PubMed: 19680289]
23. Guo X, Myasnikov AG, Chen J, Crucifix C, Papai G, Takacs M, Schultz P, Weixlbaumer A. Structural Basis for NusA Stabilized Transcriptional Pausing. Mol Cell. 2018; 69:816–827.e4. [PubMed: 29499136]
24. Brandt F, Etchells SA, Ortiz JO, Elcock AH, Hartl FU, Baumeister W. The native 3D organization of bacterial polysomes. Cell. 2009; 136:261–271. [PubMed: 19167328]
25. Turtola M, Belogurov GA. NusG inhibits RNA polymerase backtracking by stabilizing the minimal transcription bubble. elife. 2016; 5:e18096. [PubMed: 27697152]
26. Russel D, Lasker K, Webb B, Velázquez-Muriel J, Tjioe E, Schneidman-Duhovny D, Peterson B, Sali A. Putting the pieces together: integrative modeling platform software for structure determination of macromolecular assemblies. PLoS Biol. 2012; 10:e1001244. [PubMed: 22272186]
27. Beuth B, Pennell S, Arnvig KB, Martin SR, Taylor IA. Structure of a Mycobacterium tuberculosis NusA-RNA complex. EMBO J. 2005; 24:3576–3587. [PubMed: 16193062]
28. Svetlov MS, Plessa E, Chen W-C, Bougas A, Krokidis MG, Dinos GP, Polikanov YS. High-resolution crystal structures of ribosome-bound chloramphenicol and erythromycin provide the ultimate basis for their competition. RNA. 2019; 25:600–606. [PubMed: 30733327]
29. Maffioli SI, Zhang Y, Degen D, Carzaniga T, Del Gatto G, Serina S, Monciardini P, Mazzetti C, Guglierame P, Candiani G, Chiriac AI, et al. Antibacterial Nucleoside-Analog Inhibitor of Bacterial RNA Polymerase. Cell. 2017; 169:1240–1248.e23. [PubMed: 28622509]
30. Brilot AF, Korostelev AA, Ermolenko DN, Grigorieff N. Structure of the ribosome with elongation factor G trapped in the pretranslocation state. Proc Natl Acad Sci USA. 2013; 110:20994–20999. [PubMed: 24324137]
31. Halbedel S, Hames C, Stulke J. In Vivo Activity of Enzymatic and Regulatory Components of the Phosphoenolpyruvate:Sugar Phosphotransferase System in Mycoplasma pneumoniae. J Bacteriol Res. 2004; 186:7936–8943.
32. Chen ZA, Jawhari A, Fischer L, Buchen C, Tahir S, Kamenski T, Rasmussen M, Lariviere L, Bukowski-Wills J, Nilges M, Cramer P, et al. Architecture of the RNA polymerase II–TFIIF complex revealed by cross-linking and mass spectrometry. EMBO J. 2010; 29:717–726. [PubMed: 20094031]
33. Leitner A, Reischl R, Walzthoeni T, Herzog F, Bohn S, Förster F, Aebersold R. Expanding the chemical cross-linking toolbox by the use of multiple proteases and enrichment by size exclusion chromatography. Mol Cell Proteomics. 2012; 11
34. Mendes ML, Fischer L, Chen ZA, Barbon M, O'Reilly FJ, Giese SH, Bohlke-Schneider M, Belsom A, Dau T, Combe CW, Graham M, et al. An integrated workflow for crosslinking mass spectrometry. Mol Syst Biol. 2019; 15:e8994. [PubMed: 31556486]
35. Kastritis PL, O'Reilly FJ, Bock T, Li Y, Rogon MZ, Buczak K, Romanov N, Betts MJ, Bui KH, Hagen WJ, Hennrich ML, et al. Capturing protein communities by structural proteomics in a thermophilic eukaryote. Mol Syst Biol. 2017; 13:936. [PubMed: 28743795]

36. Kolbowski L, Mendes ML, Rappsilber J. Optimizing the Parameters Governing the Fragmentation of Cross-Linked Peptides in a Tribrid Mass Spectrometer. Anal Chem. 2017; 89:5311–5318. [PubMed: 28402676]
37. Stieger CE, Doppler P, Mechtler K. Optimized Fragmentation Improves the Identification of Peptides Cross-Linked by MS-Cleavable Reagents. J Proteome Res. 2019; 18:1363–1370. [PubMed: 30693776]
38. Chambers MC, Maclean B, Burke R, Amodei D, Ruderman DL, Neumann S, Gatto L, Fischer B, Pratt B, Egertson J, Hoff K, et al. A cross-platform toolkit for mass spectrometry and proteomics. Nat Biotechnol. 2012; 30:918–920. [PubMed: 23051804]
39. van Noort V, Seebacher J, Bader S, Mohammed S, Vonkova I, Betts MJ, Kühner S, Kumar R, Maier T, O'Flaherty M, Rybin V, et al. Cross-talk between phosphorylation and lysine acetylation in a genome-reduced bacterium. Mol Syst Biol. 2017; 8:571.
40. Fischer L, Rappsilber J. Quirks of Error Estimation in Cross-Linking/Mass Spectrometry. Anal Chem. 2017; 89:3829–3833. [PubMed: 28267312]
41. Schwänhausser B, Busse D, Li N, Dittmar G, Schuchhardt J, Wolf J, Chen W, Selbach M. Global quantification of mammalian gene expression control. Nature. 2011; 473:337–342. [PubMed: 21593866]
42. Karimova G, Pidoux J, Ullmann A, Ladant D. A bacterial two-hybrid system based on a reconstituted signal transduction pathway. Proc Natl Acad Sci USA. 1998; 95:5752–5756. [PubMed: 9576956]
43. Piñero-Lambea C, Garcia-Ramallo E, Martinez S, Delgado J, Serrano L, Lluch-Senar M. Mycoplasma pneumoniae Genome Editing Based on Oligo Recombineering and Cas9-Mediated Counterselection. ACS Synth Biol.
44. Mastronarde DN. Automated electron microscope tomography using robust prediction of specimen movements. J Struct Biol. 2005; 152:36–51. [PubMed: 16182563]
45. Hagen WJH, Wan W, Briggs JAG. Implementation of a cryo-electron tomography tilt-scheme optimized for high resolution subtomogram averaging. J Struct Biol. 2017; 197:191–198. [PubMed: 27313000]
46. Fukuda Y, Laugks U, Lučić V, Baumeister W, Danev R. Electron cryotomography of vitrified cells with a Volta phase plate. J Struct Biol. 2015; 190:143–154. [PubMed: 25770733]
47. Kremer JR, Mastronarde DN, McIntosh JR. Computer visualization of three-dimensional image data using IMOD. J Struct Biol. 1996; 116:71–76. [PubMed: 8742726]
48. Hrabe T, Chen Y, Pfeffer S, Cuellar LK, Mangold A-V, Förster F. PyTom: a python-based toolbox for localization of macromolecules in cryo-electron tomograms and subtomogram analysis. J Struct Biol. 2012; 178:177–188. [PubMed: 22193517]
49. Tang G, Peng L, Baldwin PR, Mann DS, Jiang W, Rees I, Ludtke SJ. EMAN2: an extensible image processing suite for electron microscopy. J Struct Biol. 2007; 157:38–46. [PubMed: 16859925]
50. Nickell S, Förster F, Linaroudis A, Net WD, Beck F, Hegerl R, Baumeister W, Plitzko JM. TOM software toolbox: acquisition and analysis for electron tomography. J Struct Biol. 2005; 149:227–234. [PubMed: 15721576]
51. Seybert A, Herrmann R, Frangakis AS. Structural analysis of Mycoplasma pneumoniae by cryo-electron tomography. J Struct Biol. 2006; 156:342–354. [PubMed: 16875842]
52. Bharat TAM, Scheres SHW. Resolving macromolecular structures from electron cryotomography data using subtomogram averaging in RELION. Nat Protoc. 2016; 11:2054–2065. [PubMed: 27685097]
53. Tegunov D, Cramer P. Real-time cryo-electron microscopy data preprocessing with Warp. Nat Methods. 2019; 16:1146–1152. [PubMed: 31591575]
54. Bharat TAM, Russo CJ, Löwe J, Passmore LA, Scheres SHW. Advances in Single-Particle Electron Cryomicroscopy Structure Determination applied to Sub-tomogram Averaging. Structure. 2015; 23:1743–1753. [PubMed: 26256537]
55. Tan YZ, Baldwin PR, Davis JH, Williamson JR, Potter CS, Carragher B, Lyumkis D. Addressing preferred specimen orientation in single-particle cryo-EM through tilting. Nat Methods. 2017; 14:793–796. [PubMed: 28671674]

56. Nakane T, Kimanius D, Lindahl E, Scheres SH. Characterisation of molecular motions in cryo-EM single-particle data by multi-body refinement in RELION. elife. 2018; 7:e36861. [PubMed: 29856314]
57. Bartesaghi A, Lecumberry F, Sapiro G, Subramaniam S. Protein secondary structure determination by constrained single-particle cryo-electron tomography. Structure. 2012; 20:2003–2013. [PubMed: 23217682]
58. Himes BA, Zhang P. emClarity: software for high-resolution cryo-electron tomography and subtomogram averaging. Nat Methods. 2018; 15:955–961. [PubMed: 30349041]
59. Zivanov J, Nakane T, Forsberg BO, Kimanius D, Hagen WJ, Lindahl E, Scheres SH. New tools for automated high-resolution cryo-EM structure determination in RELION-3. elife. 2018; 7:e42166. [PubMed: 30412051]
60. Scheres SHW. RELION: implementation of a Bayesian approach to cryo-EM structure determination. J Struct Biol. 2012; 180:519–530. [PubMed: 23000701]
61. Wang L, Shkolnisky Y, Singer A. A Fourier-based Approach for Iterative 3D Reconstruction from Cryo-EM Images. aRxiv. 2013
62. Castaño-Díez D, Kudryashev M, Arheit M, Stahlberg H. Dynamo: a flexible, user-friendly development tool for subtomogram averaging of cryo-EM data in high-performance computing environments. J Struct Biol. 2012; 178:139–151. [PubMed: 22245546]
63. Heumann JM, Hoenger A, Mastronarde DN. Clustering and variance maps for cryoelectron tomography using wedge-masked differences. J Struct Biol. 2011; 175:288–299. [PubMed: 21616153]
64. Pettersen EF, Goddard TD, Huang CC, Couch GS, Greenblatt DM, Meng EC, Ferrin TE. UCSF Chimera - a visualization system for exploratory research and analysis. J Comput Chem. 2004; 25:1605–1612. [PubMed: 15264254]
65. Goddard TD, Huang CC, Meng EC, Pettersen EF, Couch GS, Morris JH, Ferrin TE. UCSF ChimeraX: Meeting modern challenges in visualization and analysis. Protein Sci. 2018; 27:14–25. [PubMed: 28710774]
66. Naydenova K, Russo CJ. Measuring the effects of particle orientation to improve the efficiency of electron cryomicroscopy. Nat Commun. 2017; 8:629. [PubMed: 28931821]
67. Madeira F, Park YM, Lee J, Buso N, Gur T, Madhusoodanan N, Basutkar P, Tivey RNA, Potter SC, Finn RD, Lopez R. The EMBL-EBI search and sequence analysis tools APIs in 2019. Nucleic Acids Res. 2019; 47:W636–W641. [PubMed: 30976793]
68. Mészáros B, Erdos G, Dosztányi Z. IUPred2A: context-dependent prediction of protein disorder as a function of redox state and protein binding. Nucleic Acids Res. 2018; 46:W329–W337. [PubMed: 29860432]
69. Drozdetskiy A, Cole C, Procter J, Barton GJ. JPred4: a protein secondary structure prediction server. Nucleic Acids Res. 2015; 43:W389–94. [PubMed: 25883141]
70. Waterhouse AM, Procter JB, Martin DMA, Clamp M, Barton GJ. Jalview Version 2--a multiple sequence alignment editor and analysis workbench. Bioinformatics. 2009; 25:1189–1191. [PubMed: 19151095]
71. Waterhouse A, Bertoni M, Bienert S, Studer G, Tauriello G, Gumienny R, Heer FT, de Beer TAP, Rempfer C, Bordoli L, Lepore R, et al. SWISS-MODEL: homology modelling of protein structures and complexes. Nucleic Acids Res. 2018; 46:W296–W303. [PubMed: 29788355]
72. Sohmen D, Chiba S, Shimokawa-Chiba N, Innis CA, Berninghausen O, Beckmann R, Ito K, Wilson DN. Structure of the Bacillus subtilis 70S ribosome reveals the basis for species-specific stalling. Nat Commun. 2015; 6:6941. [PubMed: 25903689]
73. Ling C, Ermolenko DN. Structural insights into ribosome translocation. Wiley Interdiscip Rev RNA. 2016; 7:620–636. [PubMed: 27117863]
74. Kang JY, Mooney RA, Nedialkov Y, Saba J, Mishanina TV, Artsimovitch I, Landick R, Darst SA. Structural Basis for Transcript Elongation Control by NusG Family Universal Regulators. Cell. 2018; 173:1650–1662.e14. [PubMed: 29887376]
75. Webb B, Sali A. Comparative Protein Structure Modeling Using MODELLER. Curr Protoc Bioinformatics. 2016; 54:5.6.1–5.6.37. [PubMed: 27322406]

76. Hertig S, Goddard TD, Johnson GT, Ferrin TE. Multidomain Assembler (MDA) Generates Models of Large Multidomain Proteins. Biophys J. 2015; 108:2097–2102. [PubMed: 25954868]
77. Dauden MI, Kosinski J, Kolaj-Robin O, Desfosses A, Ori A, Faux C, Hoffmann NA, Onuma OF, Breunig KD, Beck M, Sachse C, et al. Architecture of the yeast Elongator complex. EMBO Rep. 2017; 18:264–279. [PubMed: 27974378]
78. Bonomi M, Hanot S, Greenberg CH, Sali A, Nilges M, Vendruscolo M, Pellarin R. Bayesian Weighing of Electron Cryo-Microscopy Data for Integrative Structural Modeling. Structure. 2019; 27:175–188.e6. [PubMed: 30393052]
79. Shi Y, Fernandez-Martinez J, Tjioe E, Pellarin R, Kim SJ, Williams R, Schneidman-Duhovny D, Sali A, Rout MP, Chait BT. Structural characterization by cross-linking reveals the detailed architecture of a coatomer-related heptameric module from the nuclear pore complex. Mol Cell Proteomics. 2014; 13:2927–2943. [PubMed: 25161197]
80. Viswanath S, Chemmama IE, Cimermancic P, Sali A. Assessing Exhaustiveness of Stochastic Sampling for Integrative Modeling of Macromolecular Structures. Biophys J. 2017; 113:2344–2353. [PubMed: 29211988]
81. Kosinski J, von Appen A, Ori A, Karius K, Müller CW, Beck M. Xlink Analyzer: software for analysis and visualization of cross-linking data in the context of three-dimensional structures. J Struct Biol. 2015; 189:177–183. [PubMed: 25661704]
82. Stagno JR, Altieri AS, Bubunenko M, Tarasov SG, Li J, Court DL, Andrew Byrd R, Ji X. Structural basis for RNA recognition by NusB and NusE in the initiation of transcription antitermination. Nucleic Acids Res. 2011; 39:7803–7815. [PubMed: 21652641]
83. Szklarczyk D, Gable AL, Lyon D, Junge A, Wyder S, Huerta-Cepas J, Simonovic M, Doncheva NT, Morris JH, Bork P, Jensen LJ, et al. Mering, STRING v11: protein-protein association networks with increased coverage, supporting functional discovery in genome-wide experimental datasets. Nucleic Acids Res. 2019; 47:D607–D613. [PubMed: 30476243]
84. Durand S, Gilet L, Bessières P, Nicolas P, Condon C. Three essential ribonucleases-RNase Y, J1, and III-control the abundance of a majority of Bacillus subtilis mRNAs. PLoS Genet. 2012; 8:e1002520. [PubMed: 22412379]
85. Schweimer K, Prasch S, Sujatha PS, Bubunenko M, Gottesman ME, Rösch P. NusA interaction with the α subunit of E. coli RNA polymerase is via the UP element site and releases autoinhibition. Structure. 2011; 19:945–954. [PubMed: 21742261]
86. Mah T-F, Kuznedelov K, Mushegian A, Severinov K, Greenblatt J. The α subunit of E. coli RNA polymerase activates RNA binding by NusA. Genes Dev. 2000; 14:2664–2675. [PubMed: 11040219]
87. Krupp F, Said N, Huang Y-H, Loll B, Bürger J, Mielke T, Spahn CMT, Wahl MC. Structural Basis for the Action of an All-Purpose Transcription Anti-termination Factor. Mol Cell. 2019; 74:143–157.e5. [PubMed: 30795892]
88. Chen J, Wassarman KM, Feng S, Leon K, Feklistov A, Winkelman JT, Li Z, Walz T, Campbell EA, Darst SA. 6S RNA Mimics B-Form DNA to Regulate Escherichia coli RNA Polymerase. Mol Cell. 2017; 68:388–397.e6. [PubMed: 28988932]
89. Lamour V, Westblade LF, Campbell EA, Darst SA. Crystal structure of the in vivo-assembled Bacillus subtilis Spx/RNA polymerase alpha subunit C-terminal domain complex. J Struct Biol. 2009; 168:352–356. [PubMed: 19580872]
90. 'men Abdelkareem M, Saint-André C, Takacs M, Papai G, Crucifix C, Guo X, Ortiz J, Weixlbaumer A. Structural Basis of Transcription: RNA Polymerase Backtracking and Its Reactivation. Mol Cell. 2019; 75:298–309.e4. [PubMed: 31103420]
91. Demo G, Papoušková V, Komárek J, Kadeřávek P, Otrusinová O, Srb P, Rabatinová A, Krásný L, Žídek L, Sklenář V, Wimmerová M, et al. X-ray vs. NMR structure of N-terminal domain of δ-subunit of RNA polymerase. J Struct Biol. 2014; 187:174–186. [PubMed: 24937760]

Europe PMC Funders Author Manuscripts

One Sentence Summary

Integrative in-cell structural biology provides structural insights into bacterial transcription-translation coupling.

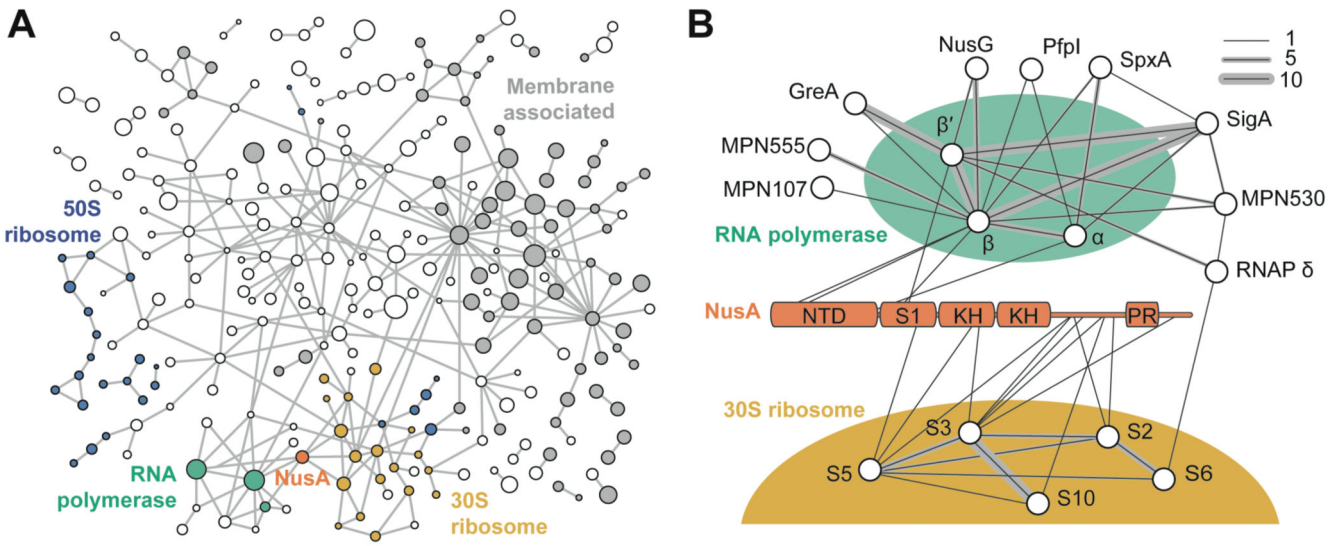

Fig. 1. Crosslink-based protein interaction map of *M. pneumoniae* proteome.

(A) 577 distinct PPIs identified at 5% PPI-level FDR (interactions to 8 abundant glycolytic enzymes and chaperones are removed for clarity). Membrane-associated proteins are shown in grey. Circle diameter indicates relative protein size. Blue: 50S ribosomal proteins; yellow: 30S ribosomal proteins; green: RNAP; orange: NusA. Each edge represents one or more crosslinks. **(B)** Interactors of RNAP and NusA. NusA NTD, S1, KH domains, and proline rich region (PR) are annotated. Line thickness represents the number of identified crosslinks.

Europe PMC Funders Author Manuscripts

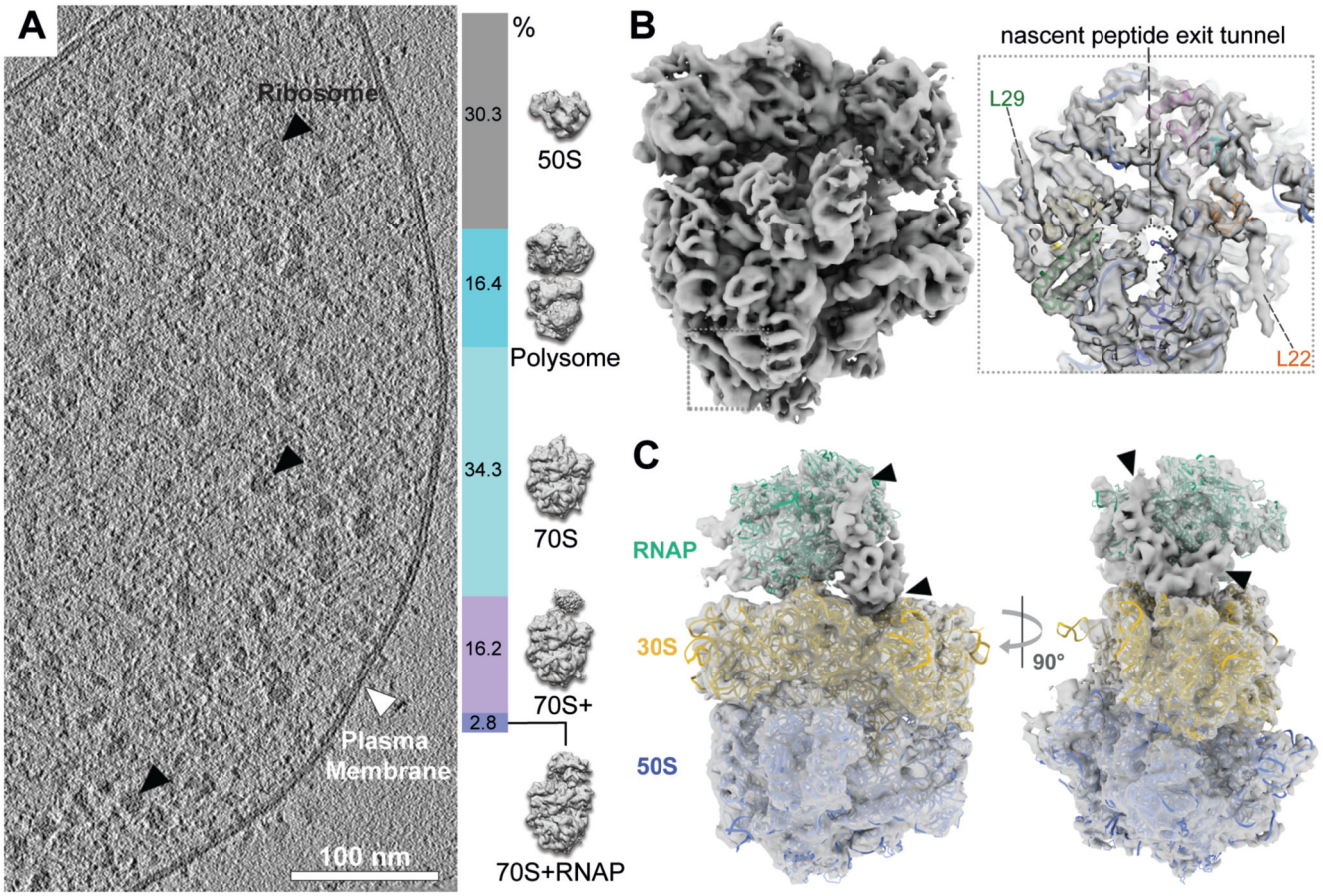

Fig. 2. In-cell cryo-ET reveals the presence of an RNAP-ribosome supercomplex.

(A) Left: tomographic slice of a *M. pneumoniae* cell. Right: classification of 108,501 ribosome sub-tomograms from *M. pneumoniae cells*. **(B)** Left: 5.6 Å in-cell 70S ribosome density. Insert: density near the peptide exit tunnel (dashed circle) shows two helices not accounted for by the fitted homology model (L22 and L29). **(C)** 9.2 Å in-cell structure of RNAP-ribosome supercomplexes (2.8% in (A)), fitted with homology models. Arrowheads indicate remaining unassigned density.

Europe PMC Funders Author Manuscripts

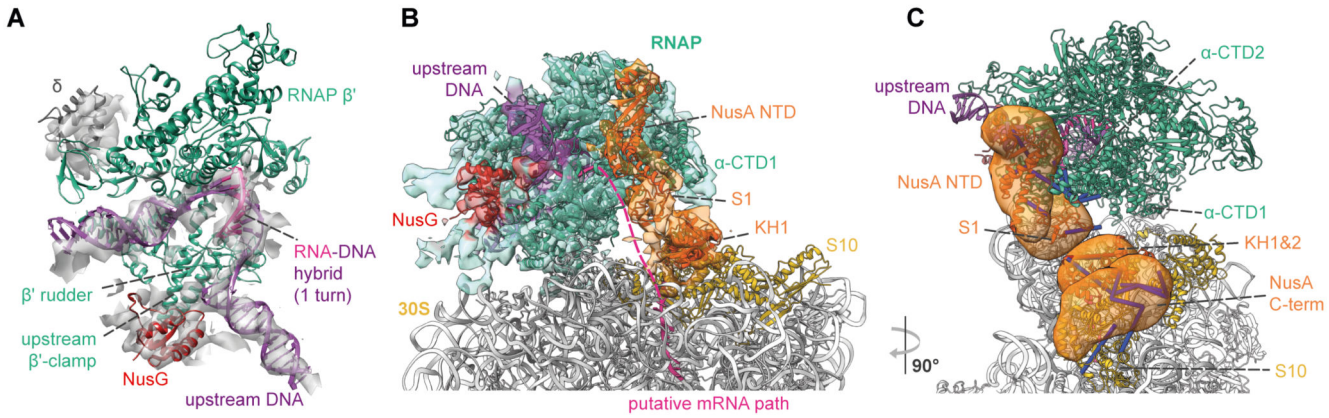

Fig. 3. Integrative model of the *M. pneumoniae* elongating expressome.

(A) Cryo-EM density of RNAP corresponding to the DNA, RNA-DNA hybrid, upstream β' clamp, δ subunit and NusG, accommodates one turn of the RNA-DNA hybrid consistent with an elongating RNAP. **(B)** Integrative model with cryo-EM density of the RNAP-NusG-NusA-ribosome elongating expressome. Structured regions are represented as colored cartoons. The electron density colors represent the subunits occupying the corresponding volumes. Coarse-grained regions are not shown. Schematic of the putative mRNA path refers to the shortest distance between mRNA exit and entry sites. **(C)** The mRNA exit tunnel face of RNAP is covered by NusA. Localization probability densities for NusA domains are shown in orange. Crosslinks between NusA and other proteins are shown. Satisfied crosslinks (<35 Å) are in blue, overlong crosslinks are in red.

Europe PMC Funders Author Manuscripts

Europe PMC Funders Author Manuscripts

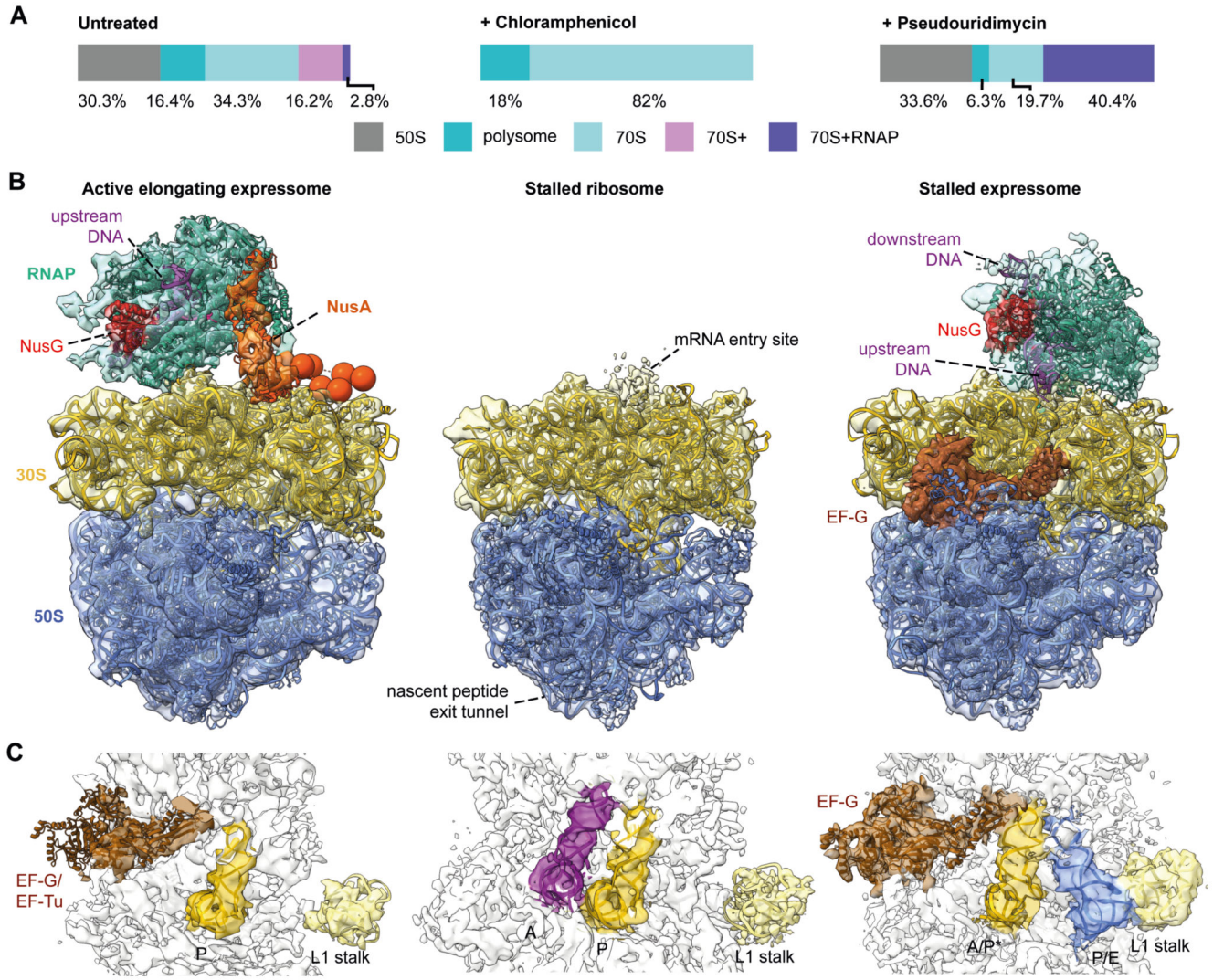

Fig. 4. Stalling translation or transcription alters the expressome architecture in cells.

(A) Classification of sub-tomograms in untreated, Cm- and PUM-treated *M. pneumoniae* cells revealed shifts in ribosome populations following perturbations. **(B)** Models of RNAP-ribosome supercomplexes and the Cm-stalled ribosome. Left: in untreated cells, the expressome compromises an actively elongating RNAP and ribosome. Center: Cm decoupled the ribosome and RNAP. Right: in PUM-treated cells, the ribosome encounters the stalled RNAP. **(C)** Ribosome tRNA occupancy states. In untreated cells, densities for P-site tRNA and elongation factors densities were visible, indicating a translating ribosome. Upon addition of Cm, A and P site tRNAs were observed indicating a stalled ribosome. In PUM-treated cells, presence of EF-G and hybrid A/P* and P/E site tRNAs suggested a pre-translocation stalled state.